Clinical Radiology 74 (2019) 816.e1–816.e8

Contents lists available at ScienceDirect

Clinical Radiology

journal homepage: www.clinicalradiologyonline.net

Differences between primary central nervous system lymphoma and glioblastoma: topographic analysis using voxel-based morphometry

K. Yamashita [a,*], A. Hiwatashi [b], O. Togao [a], K. Kikuchi [a], D. Momosaka [a], N. Hata [c], Y. Akagi [c], S.O. Suzuki [d], T. Iwaki [d], K. Iihara [c], H. Honda [a]

[a] *Department of Clinical Radiology, Graduate School of Medical Sciences, Kyushu University, 3-1-1, Maidashi, Higashi-ku, Fukuoka 812-8582 Japan*
[b] *Department of Molecular Imaging and Diagnosis, Graduate School of Medical Sciences, Kyushu University, 3-1-1, Maidashi, Higashi-ku, Fukuoka 812-8582 Japan*
[c] *Department of Neurosurgery, Graduate School of Medical Sciences, Kyushu University, 3-1-1, Maidashi, Higashi-ku, Fukuoka 812-8582 Japan*
[d] *Department of Neuropathology, Graduate School of Medical Sciences, Kyushu University, 3-1-1, Maidashi, Higashi-ku, Fukuoka 812-8582 Japan*

ARTICLE INFORMATION

Article history:
Received 8 March 2019
Accepted 26 June 2019

AIM: To evaluate the diagnostic feasibility of probabilistic analysis using voxel-based morphometry (VBM) in differentiating primary central nervous system lymphoma (PCNSL) from glioblastoma (GBM).

MATERIALS AND METHODS: In total, 118 patients with GBM (57 males, 61 females; mean [± standard deviation] age, 56.9±19.3 years; median, 61 years) and 52 patients with PCNSL (37 males, 15 females; mean age, 62±13.3 years, median, 66 years) were studied retrospectively. Each patient underwent preoperative contrast-enhanced T1-weighted imaging (CE-T1WI) using a 1.5 or 3 T magnetic resonance imaging (MRI) system. To assess preferential occurrence sites, images from CE-T1WI were co-registered and spatially normalised using the MNI152 T1 template. Subsequently, a region of interest (ROI) was placed in the centre of the enhancing tumour in normalised images with 1-mm isotropic resolution. The same ROI between normalised and T1 template images was set up using an ROI manager function in ImageJ software. A spherical volume of interest (VOI) with a radius of 10 mm was determined. A probability map was created by overlaying each image with the VOI. Each VOI was removed from T1 template images for VBM analysis. VBM analysis was performed using statistical parametric mapping (SPM) 12 software under default settings.

RESULTS: VBM analysis showed significantly higher frequency in the splenium of the corpus callosum among PCNSL patients than among GBM patients ($p<0.05$; family-wise error correction).

* Guarantor and correspondent: K. Yamashita, Department of Clinical Radiology, Graduate School of Medical Sciences, Kyushu University, 3-1-1 Maidashi, Higashi-ku, Fukuoka 812-8582, Japan. Tel.: +81 92 642 5695; fax: +81 92 642 5708.
E-mail address: yamakou@radiol.med.kyushu-u.ac.jp (K. Yamashita).

https://doi.org/10.1016/j.crad.2019.06.017

CONCLUSION: Topographic analysis using VBM provides useful information for differentiating PCNSL from GBM.

Introduction

Primary central nervous system lymphoma (PCNSL) accounts for 3–4% of newly diagnosed brain tumours and is less common than glioma.[1,2] A prominent risk factor for the development of PCNSL is immunodeficiency; however, this pathology can occur at any age, even in immunocompetent individuals, and the incidence is gradually increasing. Almost all PCNSL cases are proven to represent the diffuse large B-cell subtype on histopathological examination. Stereotactic biopsy provides sufficient information and an invasive surgical approach is unnecessary, because PCNSLs usually show chemoradiosensitive properties.

On the other hand, glioblastoma (GBM) is the most common and aggressive primary malignant brain tumour in adults. In the vast majority of cases with clinically and radiographically suspected GBM, optimal surgical resection followed by adjuvant radiotherapy plus temozolomide is the standard treatment approach. The extent of tumour resection has been shown to influence patient survival.[3,4] Pretreatment differentiation between PCNSL and GBM is thus crucial for setting appropriate management strategies.

Magnetic resonance imaging (MRI) is a key technique for non-invasive preoperative diagnosis of CNS tumours. Both PCNSL and GBM appear to be increasing rapidly, especially among elderly patients. Both lesions are usually seen as strongly enhancing masses on MRI, often accompanied by surrounding oedema.

Several imaging parameters obtained from advanced MRI provide useful quantitative information for non-invasively distinguishing between PCNSL and GBM, including regional tumour blood flow from arterial spin labelling[5–7]; tumour blood volume given by dynamic susceptibility contrast[5] or dynamic contrast-enhanced imaging[5,8]; apparent diffusion coefficient (ADC) measured on diffusion-weighted imaging[6,8–12]; and combined true diffusion coefficient with perfusion fraction derived from intravoxel incoherent motion imaging.[13] Another well-known approach to evaluating malignant tumour is 2-[^{18}F]-fluoro-2-deoxy-D-glucose (FDG)-positron emission tomography (PET). Increased glucose metabolism correlates with FDG accumulation, which is useful in distinguishing PCNSL from GBM.[6]

In contrast, there have been no studies to evaluate tumour location for distinguishing between PCNSL and GBM. Tumour location offers important information not only for diagnosing CNS tumour, but also for determining resection rates and patient outcomes. The correlation between *isocitrate dehydrogenase* (*IDH*) mutation status and tumour location has been reported in the literature. For example, gliomas with mutant *IDH*, probably due to oligodendroglioma or oligo components, tend to be located in the frontal lobe.[14–16]

Voxel-based morphometry (VBM) has the advantage of assessing the whole brain and not being biased to one particular region or structure. This method entails a voxel-wise comparison of local volumes of grey and white matter between groups after images are spatially normalised into the same space, segmented, modulated, and smoothed.[17,18] VBM has been reported to be useful in distinguishing neurodegenerative diseases such as Alzheimer's disease,[19] Parkinson's disease,[20] and frontotemporal dementia.[21] On the other hand, the utility of discrimination between PCNSL and GBM has not yet been explored. Therefore, the purpose of the present study was to evaluate the diagnostic feasibility of topographic analysis using VBM in differentiating PCNSL from GBM.

Materials and methods

Patients

This study was approved by the institutional review board and informed consent for study participation was waived due to the retrospective nature of this study. MRI data for consecutive patients from January 2003 to May 2016 were obtained and retrospectively analysed (Electronic Supplementary Material) Cases with recurrent GBMs were excluded. Consequently, data for 52 patients with PCNSL (37 men, 15 women; median age, 66 years; range 22–86 years) and 118 patients with GBM (57 men, 61 women; median age, 61 years; range 3–84 years) were examined. All PCNSLs and GBMs were diagnosed histopathologically by experienced neuropathologists. The mean interval between MRI and surgery was 6.1 days (range, 0–21 days).

MRI

MRI images were obtained using a 1.5 or 3 T MRI unit. Each patient underwent preoperative pre- and post-contrast transverse T1-weighted imaging. The details for MRI units and acquisition parameters are listed in Table 1. A standard dose (0.2 ml/kg body weight) of gadolinium-based contrast agent, gadopentate dimeglumine (Magnevist; Bayer Yakuhin, Osaka, Japan), gadoteridol (ProHance; Eisai, Tokyo, Japan), gadodiamide (Omniscan; Daiichi Sankyo, Tokyo, Japan), or 0.1 mL/kg body weight of gadobutol (Gadovist; Bayer Yakuhin), was injected intravenously.

Table 1
Imaging protocols for pre- and post-contrast T1-weighted imaging (T1WI).

	1.5 T		3 T	
	Vision (n=25)	Symphony (n=11)	Achieva (n=125)	Ingenia (n=9)
Pre-contrast T1WI				
TR/TE (ms)	493-551/11-14	493-494/11	400-424/10	450-452/8.7–9
Flip angle (°)	90	80	90	75
Matrix	512×192	256×192-208	256×217	256×205
Field of view	230×230	172.5-230×230	230×230	230×230
Section thickness/gap (mm)	5/2.5	5/2.5	5/1	5/1
Post-contrast T1WI				
TR/TE (ms)	541-636/17	541-624/17	400-498/17-20	440-480/21
Flip angle (°)	90	80	90	75
Matrix	512×192	256×192-208	256×217	256×205
Field of view	230×230	172.5-230×230	230×230	230×230
Section thickness/gap (mm)	5/2.5	5/2.5	5/1	5/1

TR/TE, repetition time/echo time.

Image pre-processing

Post-contrast T1-weighted images were co-registered and spatially normalised using the Montreal Neurological Institute (MNI) 152 T1 template. The centre and total of enhancing tumour were determined by one author (with 16 years of experience in neuroradiology) in normalised images. When multifocal lesions were observed, the maximum enhancing lesion was targeted. The same point between normalised and T1 template images was set up using the region-of-interest (ROI) manager function of ImageJ software (version 1.48v; National Institutes of Health, Bethesda, MD, USA). Subsequently, a spherical volume-of-interest (VOI) with a radius of 10-mm was placed around the point (centre of the enhancing tumour) in the MNI template images with 1-mm isotropic resolution[22] using MRIcro (Chris Rorden, Neuropsychology Lab., Columbia, SC, USA). Each VOI was removed from the MNI template images for VBM analysis to assess the sites of preferential occurrence of PCNSL and GBM (Fig 1).

Image analysis

First, the tumour volume was carefully determined by manually outlining enhancing contours on each section with reference to images from both pre- and post-contrast T1WI, including the inside necrotic (non-enhancing) area. These determinations were performed by a board-certified neuroradiologist. When multifocal lesions were noted, the lesion showing maximum enhancement was targeted. The tumour volume was compared between PCNSL and GBM using the Mann–Whitney *U*-test. A value of $p<0.05$ was considered to indicate statistical significance. The performance in discriminating between PCNSL and GBM patients was evaluated using receiver operating characteristic analysis.

Second, probability atlases of both PCNSL and GBM were created by overlaying (the centre and total of tumour) VOIs on MRI data from each patient. Subsequently, VBM analysis was performed using Statistical Parametric Mapping software (SPM12; http://www.fil.ion.ucl.ac.uk/spm/software/spm12), implemented in the MATLAB programming environment (R2014b; MathWorks, Natick, MA, USA). Spatial normalisation was performed using the diffeomorphic anatomical registration through exponentiated lie algebra (DARTEL) algorithm, which offers highly accurate spatial normalisation based on non-linear deformation.[19] Within the normalisation procedure, data were modulated to preserve the total amount of signal in the images. All images were smoothed with a Gaussian kernel of 8 mm full-width at half-maximum. Voxel-wise statistical comparisons of PCNSL and GBM were thus performed to evaluate differences in preferential occurrence site between PCNSL and GBM. Multiple comparison corrections were performed using family-wise error (FWE) correction. A statistical threshold of $p<0.05$ was applied.

Results

A total of 112 patients of GBM had wild-type *IDH1* and six patients had mutant *IDH1*. All PCNSL patients were diagnosed with diffuse large B-cell type. The tumour volume was significantly larger in patients with GBM (32.9±30.8 cm^3; range, 0.08–179.5 cm^3) than in patients with PCNSL (15.6±16.6 cm^3; range, 0.34–79.9 cm^3; $p<0.0001$; Fig 2). The optimal cut-off value was 21.6 cm^3 with 85.4% sensitivity, 45.5% specificity, and 64.7% accuracy. The area under the curve was 0.696.

Probability atlases show that GBMs involve the periventricular white matter with high frequency (Fig 3a), whereas PCNSLs have a tendency to encompass the splenium of the corpus callosum (Fig 3b). Both PCNSLs and GBMs commonly present in supratentorial locations.

SPM analysis revealed a significantly higher frequency in the splenium of the corpus callosum for PCNSL than for GB ($p<0.05$; FWE correction; cluster size, 131; MNI coordinates of peak voxels: 1.5 mm, −42 mm, 19.5 mm; T-value, 5.17; Fig 4) with the centre of the tumour. No significant decrease in voxels in GBM (significantly higher frequency of GBM than PCNSL) was seen even using uncorrected statistics. In addition, no significant difference was observed between GBM and PCNSL with entire tumour volume. Figs 5 and 6 show representative cases of PCNSL and GBM.

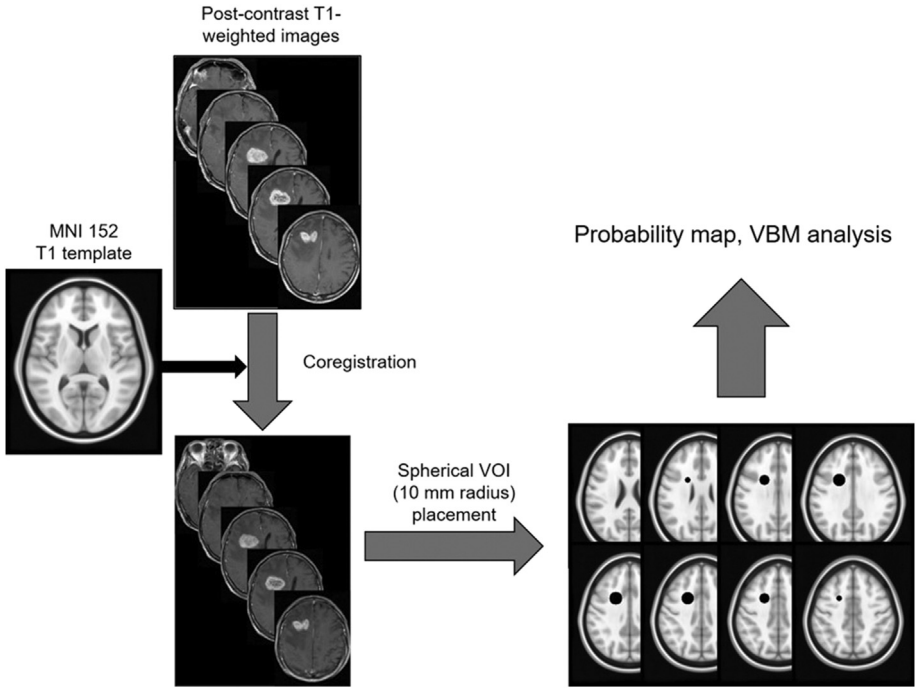

Figure 1 Image pre-processing steps. First, post-contrast T1-weighted images are co-registered and spatially normalised using the MNI152 T1 template. The centre of the enhancing tumour is then determined in normalised images. Subsequently, a spherical volume of interest (VOI) with a radius of 10-mm was placed around the point (centre of the enhancing tumour) in the MNI152 T1 template with a 1-mm isotropic resolution. Each VOI is removed from MNI152 T1 template images for VBM analysis to assess preferential sites of occurrence of PCNSL and GBM. The VOI of the entire enhancing tumour is also obtained.

Discussion

In the present study, probabilistic analysis shows that occurrence in the splenium of the corpus callosum is significantly higher for PCNSL than for GBM. The literature has reported that GBMs tend toward higher vascularity than PCNSL according to perfusion-weighted MRI.[5–8,13,23] In addition, ADC values tend to be higher for GBM than for PCNSL, probably in keeping with the differences in cellularity.[6,9–11] PCNSLs are well-known to have high glucose consumption rates, which may result in elevated glucose metabolism compared with GBM using FDG-PET.[6] The present results suggest that topographic analysis may provide additional information to distinguish between GBM and PCNSL.

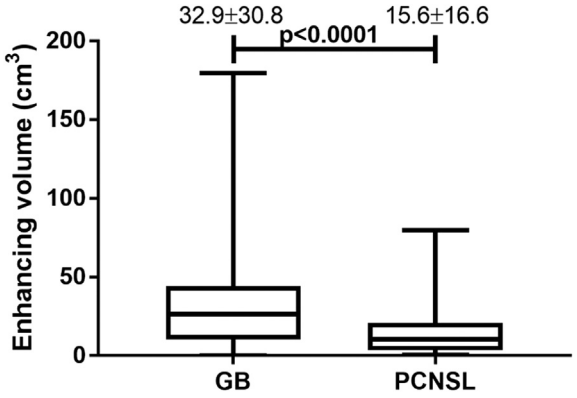

Figure 2 Box plots of tumour volume in GBM and PCNSL patients. Tumour volume is significantly larger in patients with GBM than in patients with PCNSL ($p<0.0001$).

The tendency of PCNSL to encompass the splenium of the corpus callosum represents a unique finding in the present study. The corpus callosum is made up of dense myelinated fibres.[24,25] The mechanism underlying the affinity of PCNSL for the corpus callosum still remains unclear. Bühring *et al.* pointed out that bulky infiltration of the corpus callosum unaccompanied by necrosis is suggestive of PCNSL.[26] Bruno *et al.* reported that PCNSL cases in the splenium of the corpus callosum more frequently involved mutation of the *telomerase reverse transcriptase* (*TERT*) promotor.[27] Gene mutation analysis may shed light on the tumorigenesis of PCNSL in the future, although genetic analysis of PCNSL was not performed in the present study. Probability atlases show that the location of PCNSL is variable. Thus, radiologists should pay attention to wide variety of MRI findings for PCNSL.

Probability atlases show that both GBMs and PCNSLs present commonly in the supratentorial location. GBMs involve the periventricular white matter with high frequency. The subventricular zone (SVZ) is a vulnerable site for tumour formation because it holds potentially transformable neural stem cells and may provide a perivascular niche that supports tumorigenesis.[28] The presence of SVZ involvement in GBM shows higher recurrence rates and is associated with increased tumour size and decreased

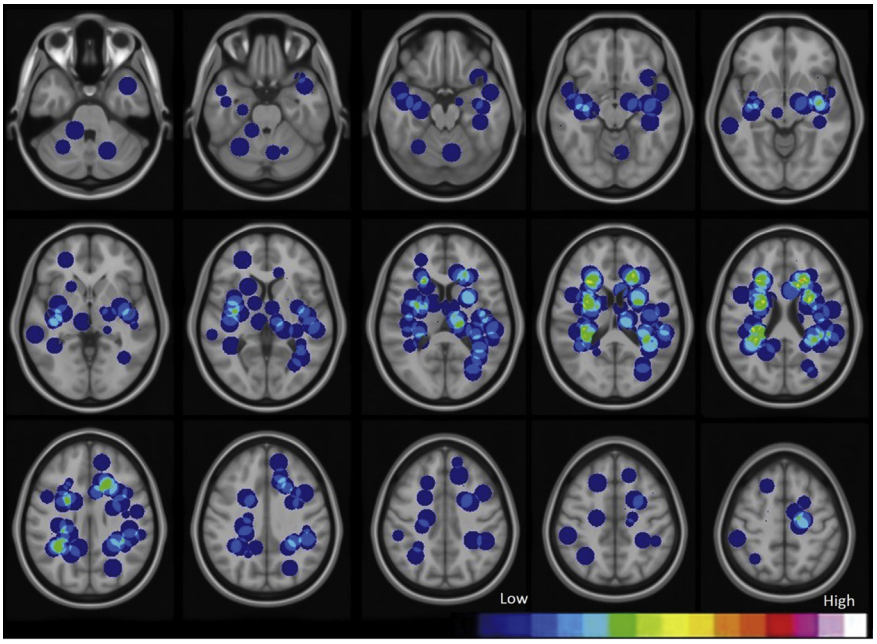

(a)

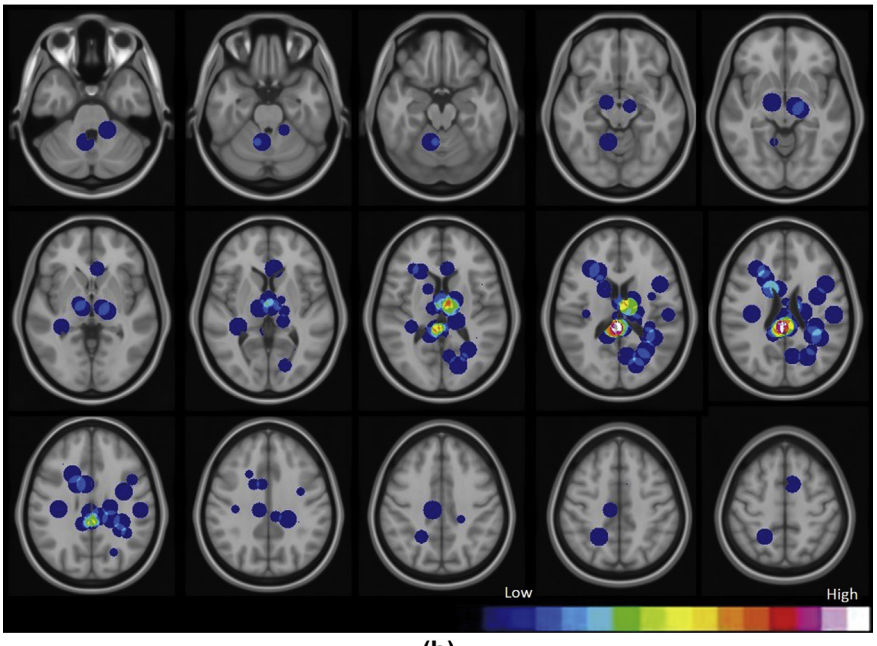

(b)

Figure 3 Probability atlases of GBM (a) and PCNSL (b). GBMs involve the periventricular white matter with high frequency, whereas PCNSLs tend to encompass the splenium of the corpus callosum. Both GBMs and PCNSLs commonly present in supratentorial locations.

survival.[28,29] In contrast, Toh *et al.* indicated that GBMs may originate from the cortical grey matter and extend into the subcortical white matter, but also emphasised a subset of GBMs that originate in the cortex and are probably from a different cell origin than periventricular or deep white matter GBMs.[30] The pathogenesis of GBM development is extremely complicated and different molecular mechanisms may underlie the evolution between cortical and SVZ origins.

The present study demonstrated that the tumour volume was significantly larger in GBM patients than in PCNSL patients. The tumour enhancement volume depends on the status of the blood–brain barrier, which is affected by tumour type.[31] In addition, the evolution of local necrosis resulted in increased tumour volume.[31] The characteristic histological appearance of GBM includes nuclear polymorphism, high mitotic activity, prominent microvascular proliferation, and/or necrosis. These facts might result in the large enhancing volume in GBM. A large standard deviation of the tumour volume in the patients with GBM was shown in the present study, suggesting a wide distribution in the tumour volume of GBM. GBM is

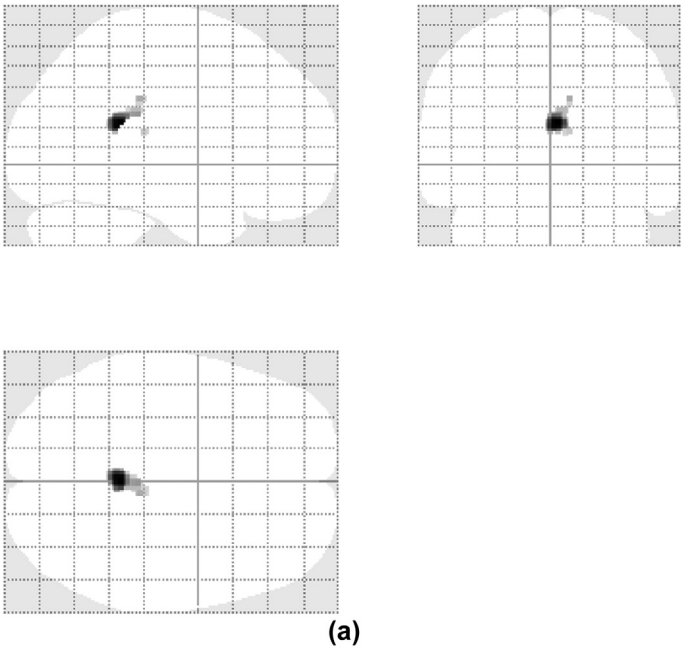

(a)

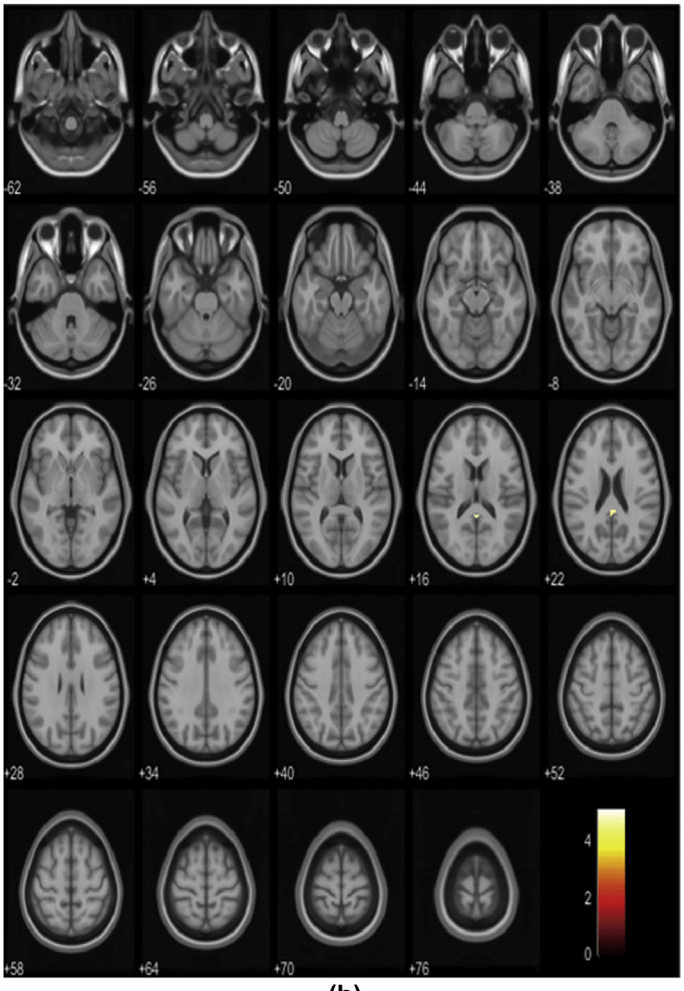

(b)

Figure 4 Maximum intensity projection images (a) and slice overlay images (b) from SPM analysis. These images reveal significantly higher frequency in the splenium of the corpus callosum among PCNSL patients than among GBM patients ($p<0.05$).

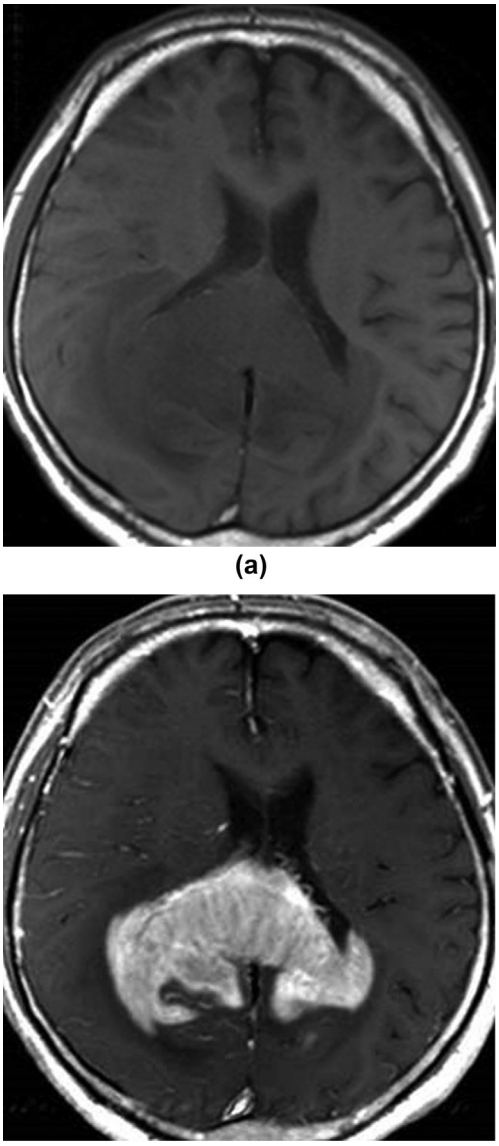

(a)

(b)

Figure 5 Pre- (a) and post-contrast-enhanced T1WI (b) of a 64-year-old man with PCNSL. The tumour is located mainly in the splenium of the corpus callosum. The tumour shows homogeneous enhancement.

characterised by inter- and intratumoural heterogeneity, which may be driven by the activation of epidermal growth factor receptor (EGFR).[32] The present results may reflect the variability of tumour cell behaviour and aggressiveness in GBM.

The present study has some limitations. First, the centre of the enhancing mass is not always the origin of the tumour. Ellingson *et al.* reported that the VOI of entire GBM presents the geographic distribution of the tumours well[14]; however, the distribution may depend on the scanning period of MRI especially at the tumour border. Comprehension of "tumour core" is one of the most important factors to distinguish PCNSL from GBM for clinical use. Second, wild-type and mutant *IDH1* were not analysed separately; however, previous reports have revealed that GBM patients with mutant IDH preferentially located in the

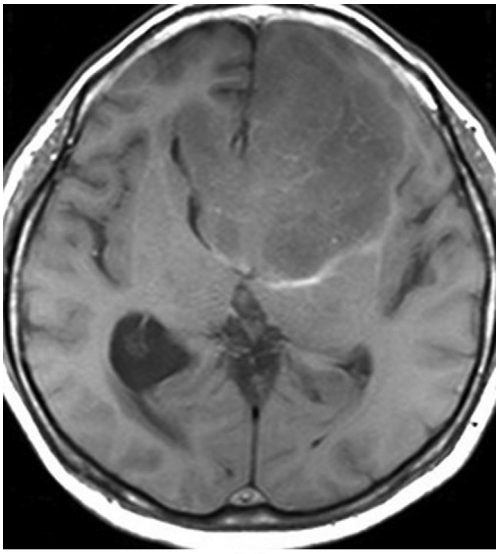

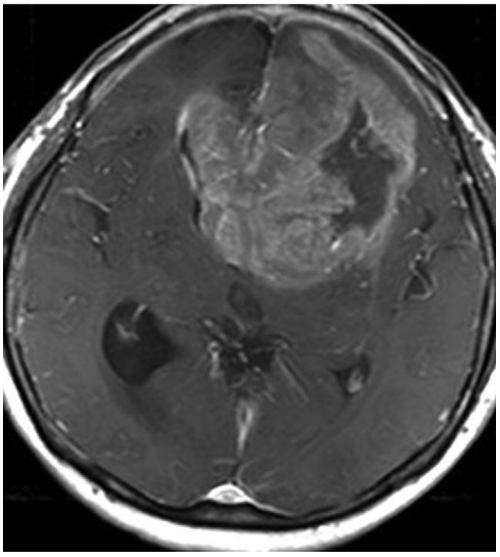

Figure 6 Pre- (a) and post-contrast-enhanced T1WI (b) of a 60-year-old man with GBM. A large enhancing volume (124.7 cm^3) is shown in the left frontal lobe. Images also demonstrate tumour necrosis.

frontal lobe[33] or insular cortex region.[34] These sites are apart from the splenium of the corpus callosum that PCNSLs involve with high frequency in the present study. Finally, comparisons of ADC, parameters derived from perfusion-weighted images, and FDG-PET were not performed because the imaging protocols and MRI units varied across patients. The present results provide the potential utility of location analysis using VBM after understanding the mainstay of advanced MRI. Dominance of splenic involvement is demonstrated with PCNSL and this might influence clinical decision-making. The next step will be to develop comprehensive approaches with the combination of advanced MRI data for non-invasive differentiation between PCNSL and GBM.

In conclusion, topographic analysis using VBM offers useful information to distinguish between GBM and PCNSL.

Conflict of interest

The authors declare no conflict of interest.

Appendix A. Supplementary data

Supplementary data to this article can be found online at https://doi.org/10.1016/j.crad.2019.06.017.

References

1. Schaff LR, Grommes C. Updates on primary central nervous system lymphoma. *Curr Oncol Rep* 2018;**20**(2):11.
2. Villano JL, Koshy M, Shaikh H, *et al*. Age, gender, and racial differences in incidence and survival in primary CNS lymphoma. *Br J Cancer* 2011;**105**(9):1414–8.
3. Pichlmeier U, Bink A, Schackert G, *et al*. Resection and survival in glioblastoma multiforme: an RTOG recursive partitioning analysis of ALA study patients. *Neuro-oncology* 2008;**10**(6):1025–34.
4. Kuhnt D, Becker A, Ganslandt O, *et al*. Correlation of the extent of tumour volume resection and patient survival in surgery of glioblastoma multiforme with high-field intraoperative MRI guidance. *Neuro-oncology* 2011;**13**(12):1339–48.
5. Weber MA, Zoubaa S, Schlieter M, *et al*. Diagnostic performance of spectroscopic and perfusion MRI for distinction of brain tumours. *Neurology* 2006;**66**(12):1899–906.
6. Yamashita K, Yoshiura T, Hiwatashi A, *et al*. Differentiating primary CNS lymphoma from glioblastoma multiforme: assessment using arterial spin labeling, diffusion-weighted imaging, and (1)(8)F-fluorodeoxyglucose positron emission tomography. *Neuroradiology* 2013;**55**(2):135–43.
7. Abdel Razek AAK, El-Serougy L, Abdelsalam M, *et al*. Differentiation of primary central nervous system lymphoma from glioblastoma: quantitative analysis using arterial spin labeling and diffusion tensor imaging. *World Neurosurg* 2019;**123**:e303–9.
8. Lin X, Lee M, Buck O, *et al*. Diagnostic accuracy of T1-weighted dynamic contrast-enhanced MRI and DWI-ADC for differentiation of glioblastoma and primary cns lymphoma. *AJNR Am J Neuroradiol* 2017;**38**(3):485–91.
9. Doskaliyev A, Yamasaki F, Ohtaki M, *et al*. Lymphomas and glioblastomas: differences in the apparent diffusion coefficient evaluated with high b-value diffusion-weighted magnetic resonance imaging at 3T. *Eur J Radiol* 2012;**81**(2):339–44.
10. Guo AC, Cummings TJ, Dash RC, *et al*. Lymphomas and high-grade astrocytomas: comparison of water diffusibility and histologic characteristics. *Radiology* 2002;**224**(1):177–83.
11. Toh CH, Castillo M, Wong AM, *et al*. Primary cerebral lymphoma and glioblastoma multiforme: differences in diffusion characteristics evaluated with diffusion tensor imaging. *AJNR Am J Neuroradiol* 2008;**29**(3):471–5.
12. Yamasaki F, Kurisu K, Satoh K, *et al*. Apparent diffusion coefficient of human brain tumours at MRI. *Radiology* 2005;**235**(3):985–91.
13. Yamashita K, Hiwatashi A, Togao O, *et al*. Diagnostic utility of intravoxel incoherent motion MRI in differentiating primary central nervous system lymphoma from glioblastoma multiforme. *J Magn Reson Imaging* 2016;**44**(5):1256–61.
14. Ellingson BM, Lai A, Harris RJ, *et al*. Probabilistic radiographic atlas of glioblastoma phenotypes. *AJNR Am J Neuroradiol* 2013;**34**(3):533–40.
15. Wang Y, Zhang T, Li S, *et al*. Anatomical localization of isocitrate dehydrogenase 1 mutation: a voxel-based radiographic study of 146 low-grade gliomas. *Eur J Neurol* 2015;**22**(2):348–54.
16. Zlatescu MC, TehraniYazdi A, Sasaki H, *et al*. Tumour location and growth pattern correlate with genetic signature in oligodendroglial neoplasms. *Cancer Res* 2001;**61**(18):6713–5.
17. Ashburner J, Friston KJ. Voxel-based morphometry—the methods. *NeuroImage* 2000;**11**(6 Pt 1):805–21.
18. Stonnington CM, Tan G, Kloppel S, *et al*. Interpreting scan data acquired from multiple scanners: a study with Alzheimer's disease. *NeuroImage* 2008;**39**(3):1180–5.

19. Dashjamts T, Yoshiura T, Hiwatashi A, *et al*. Alzheimer's disease: diagnosis by different methods of voxel-based morphometry. *Fukuoka Igaku Zasshi* 2012;**103**(3):59–69.
20. Price S, Paviour D, Scahill R, *et al*. Voxel-based morphometry detects patterns of atrophy that help differentiate progressive supranuclear palsy and Parkinson's disease. *NeuroImage* 2004;**23**(2):663–9.
21. Chang JL, Lomen-Hoerth C, Murphy J, *et al*. A voxel-based morphometry study of patterns of brain atrophy in ALS and ALS/FTLD. *Neurology* 2005;**65**(1):75–80.
22. Takano K, Kinoshita M, Takagaki M, *et al*. Different spatial distributions of brain metastases from lung cancer by histological subtype and mutation status of epidermal growth factor receptor. *Neuro-oncology* 2016;**18**(5):716–24.
23. Razek A, El-Serougy L, Abdelsalam M, *et al*. Differentiation of residual/recurrent gliomas from postradiation necrosis with arterial spin labeling and diffusion tensor magnetic resonance imaging-derived metrics. *Neuroradiology* 2018;**60**(2):169–77.
24. Bourekas EC, Varakis K, Bruns D, *et al*. Lesions of the corpus callosum: MRI and differential considerations in adults and children. *AJR Am J Roentgenol* 2002;**179**(1):251–7.
25. Kuker W, Nagele T, Korfel A, *et al*. Primary central nervous system lymphomas (PCNSL): MRI features at presentation in 100 patients. *J Neuro-Oncology* 2005;**72**(2):169–77.
26. Buhring U, Herrlinger U, Krings T, *et al*. MRI features of primary central nervous system lymphomas at presentation. *Neurology* 2001;**57**(3):393–6.
27. Bruno A, Alentorn A, Daniau M, *et al*. TERT promoter mutations in primary central nervous system lymphoma are associated with spatial distribution in the splenium. *Acta Neuropathol* 2015;**130**(3):439–40.
28. Achanta P, Sedora Roman NI, Quinones-Hinojosa A. Gliomagenesis and the use of neural stem cells in brain tumour treatment. *Anticancer Agents Med Chem* 2010;**10**(2):121–30.
29. Jafri NF, Clarke JL, Weinberg V, *et al*. Relationship of glioblastoma multiforme to the subventricular zone is associated with survival. *Neuro-oncology* 2013;**15**(1):91–6.
30. Toh CH, Castillo M. Early-stage glioblastomas: MRI-based classification and imaging evidence of progressive growth. *AJNR Am J Neuroradiol* 2017;**38**(2):288–93.
31. Donahue KM, Krouwer HG, Rand SD, *et al*. Utility of simultaneously acquired gradient-echo and spin-echo cerebral blood volume and morphology maps in brain tumour patients. *Magn Reson Med* 2000;**43**(6):845–53.
32. Lindberg OR, McKinney A, Engler JR, *et al*. GBM heterogeneity as a function of variable epidermal growth factor receptor variant III activity. *Oncotarget* 2016;**7**(48):79101–16.
33. Lai A, Kharbanda S, Pope WB, *et al*. Evidence for sequenced molecular evolution of IDH1 mutant glioblastoma from a distinct cell of origin. *J Clin Oncol* 2011;**29**(34):4482–90.
34. Hata N, Hatae R, Yoshimoto K, *et al*. Insular primary glioblastomas with IDH mutations: clinical and biological specificities. *Neuropathology* 2017;**37**(3):200–6.